Roughness-Induced Vehicle Energy Dissipation: Statistical Analysis and Scaling

ROUGHNESS–INDUCED VEHICLE ENERGY DISSIPATION: STATISTICAL ANALYSIS AND SCALING

Arghavan Louhghalam[1], A.M.ASCE

Mazdak Tootkaboni[2], A.M.ASCE

Franz-Josef Ulm[3], M.ASCE

[1]Postdoctoral Researcher, Department of Civil & Environmental Engineering, Massachusetts Institute of Technology, Cambridge MA 02139, Email: arghavan@mit.edu

[2]Assistant Professor, Department of Civil & Environmental Engineering, University of Massachusetts Dartmouth, Dartmouth MA 02747, Email: mtootkaboni@umassd.edu

[3]George Macomber Professor, Department of Civil & Environmental Engineering, Massachusetts Institute of Technology, Cambridge MA 02139, Email: ulm@mit.edu

ABSTRACT

The energy dissipated in vehicle's suspension system due to road roughness affects rolling resistance and the resulting fuel consumption and greenhouse gas emission. The key parameters driving this dissipation mechanism are identified via dimensional analysis. A mechanistic model is proposed that relates vehicle dynamic properties and road roughness statistics to vehicle dissipated energy and thus fuel consumption. Scaling relationship between the dissipated energy and the most commonly used road roughness index, International Roughness Index (IRI), is also established. It is shown that the dissipated energy scales with IRI squared and scaling of dissipation with vehicle speed V depends on road waviness number

w in the form of V^{w-2}. The effect of marginal probability distribution of road roughness profile on dissipated energy is examined. It is shown that while the marginal distribution of road profile does not affect the identified scaling relationships, the multiplicative factor in these relationships does change from one distribution to another. As an example of practical application, the model is calibrated with the empirical HDM-4 model for different vehicle classes.

Keywords: roughness-induced dissipation, pavement vehicle interaction, IRI, roughness power spectral density, stationary stochastic process, translation process theory

INTRODUCTION

Pavement roughness affects rolling resistance (Beuving et al., 2004), and thus vehicle fuel consumption. In fact, when a vehicle travels at constant speed on an uneven road surface, the mechanical work dissipated in the vehicle's suspension system is compensated by vehicle engine power, resulting in excess fuel consumption. In addition to pavement texture effects (Sandberg et al. (2011)) and viscoelastic dissipation in the pavement material (see e.g., Pouget et al. (2011), Akbarian et al. (2012), Louhghalam et al. (2013), Louhghalam et al. (2014b)), pavement roughness manifesting itself as surface unevenness with wavelengths above 50 mm (Flintsch et al., 2003), has been recognized as a main contributor to Pavement Vehicle Interactions (PVI) affecting vehicle operating costs (VOC) (Zaabar and Chatti (2010)). While the phenomenon is well known, the intricate links between road roughness parameters, vehicle dynamic characteristics, and vehicle speed remain yet to be established. The mechanistic model developed herein, aims at quantitatively assessing the impact of these parameters on roughness-induced vehicle fuel consumption and the relating greenhouse gas emission. Such models are in high demand for evaluating the environmental footprint of pavement structures during their use-phase, contributing to the development of a quantitative frameworks for pavement sustainable design and maintenance. The developments presented in this paper aim at contributing to the growing field of mechanics-based quantitative engineering sustainability. In contrast to empirical approaches, the originality of the approach herein developed relies on a combination of a thermodynamic quantity (energy dissipation) with results from random vibration theory in order to identify scaling relations of roughness-induced vehicle energy dissipation.

To motivate the forthcoming developments, consider the classical two-degree-of-freedom (2-DOF) quarter-car model (Sayers (1995)) shown in Figure 1: a two-mass system in series composed of a tire (stiffness k_t) and a spring-dashpot parallel suspension unit (stiffness k_s and viscosity coefficient C_s). We are interested in the dissipation rate (δD) of mechanical work into heat form due to the relative motion, $\dot{z} = dz/dt$ (with z the relative displacement of sprung mass m_s with respect to the unsprung mass m_u) of the suspension unit. This dissipation depends on the vehicles dynamic properties $(m_s, m_u, k_t, k_s, C_s)$, the vehicle speed V; and parameters that quantify the pavement roughness. This roughness, ξ, is typically assessed by longitudinal profile data, and condensed, after Fourier transformation, into the power spectral density (PSD) of roughness which describes the distribution of roughness across various wavenumbers (Ω) in the form of $S_\xi(\Omega) = c\Omega^{-w}$, where c is the unevenness index and w is the waviness number (Dodds and Robson (1973), Robson (1979), Kropac and Mucka (2008)). We thus seek a relationship between the dissipation per distance traveled ($\delta\mathcal{E} = \delta D/V$) and these parameters; that is:

$$\delta\mathcal{E} = \frac{C_S \dot{z}^2}{V} = f\left(m_s, m_u, k_t, k_s, C_s, V, c, \Omega_i\right) \tag{1}$$

It is useful to perform a dimensional analysis of Eq. (1) by considering an extended base dimension system ($L_x L_z M T$) that considers, in addition to mass (M) and time (T), two independent characteristic length dimensions, one for the driving direction (L_x), the other for the vertical direction of vehicle motion (L_z). For instance, in this extended base dimension system, the dissipation per lane mile traveled δD has dimension $[\delta\mathcal{E}] = [\delta D/V] = [F_z]\,[dz/dt]\,[V]^{-1} = L_x^{-1} L_z^2 M T^{-2}$ (where F_z stands for the force in the dashpot); while the speed has dimension $[V] = L_x T^{-1}$. Similarly, we obtain $[k_t] = [k_s] = MT^{-2}$, $[C_s] = MT^{-1}$, $[\Omega_i] = L_x^{-1}$, whereas for the unevenness index $[c] = [S_\xi]\,[\Omega^w] = L_x^{1-w} L_z^2$, since $[S_\xi(\Omega)] = L_x L_z^2$. The exponent matrix of dimension reads for the problem thus defined:

$$
\begin{array}{c||ccccccccc}
 & [\delta\mathcal{E}] & [m_s] & [m_u] & [k_t] & [k_s] & [C_s] & [V] & [c] & [\Omega_i] \\
\hline
L_x & -1 & 0 & 0 & 0 & 0 & 0 & 1 & 1-w & -1 \\
L_z & 2 & 0 & 0 & 0 & 0 & 0 & 0 & 2 & 0 \\
M & 1 & 1 & 1 & 1 & 1 & 1 & 0 & 0 & 0 \\
T & -2 & 0 & 0 & -2 & -2 & -1 & -1 & 0 & 0
\end{array}
\tag{2}
$$

The rank of the matrix which characterizes the number of dimensionally independent parameters, is $k = 4$ independent of the value of w. This allows one, according to the PI-Theorem (Buckingham (1914)), to reduce the dimensional problem defined by Eq. (1) to a dimensionless relation of the form:

$$
\frac{\delta\mathcal{E}}{c C_s V^{w-2} \omega_s^{3-w}} = F\left(\gamma = \frac{m_u}{m_s}, \beta = \frac{\omega_u}{\omega_s}, \zeta = \frac{C_s}{2 m_s \omega_s}, \overline{\omega}_i = \frac{\omega_i}{\omega_s}\right) \tag{3}
$$

where $\omega_u = \sqrt{k_t/m_u}$ and $\omega_s = \sqrt{k_s/m_s}$ are the natural frequency of respectively the unsprung and the sprung masses, whereas $\omega_i = V\Omega_i$ stands for the angular frequencies. The dimensional analysis is able to isolate –on the left-hand-side of Eq. (3)– the impact of pavement roughness (captured by the unevenness index c and the waviness number w) on the dissipation, from the dimensionless dynamic vehicle properties on the right-hand-side, namely mass-ratio $\gamma = m_u/m_s$, natural frequency ratio $\beta = \omega_u/\omega_s$, and damping ratio $\zeta = C_s/\left(2m\omega_s\right)$. Specifically, it reveals that the energy dissipation scales with the vehicle speed as $\delta\mathcal{E} \propto V^{w-2}$. That is, for waviness numbers $w > 2$, the dissipated energy increases with the vehicle speed, and for values $w < 2$, it is the inverse.

With the problem thus defined, the focus of the rest of this paper is to quantify by means of a mechanistic modeling the relationship between vehicle properties and road roughness statistics, and the dimensionless roughness-induced energy dissipation.

ROUGHNESS-INDUCED DISSIPATION

Since road roughness ξ is random, the suspension motion and consequently energy dissipation in Eq. (1) are stochastic quantities. Modeling road roughness and suspension motion as stochastic processes defined in space and time, Eq. (1) is rewritten in the form:

$$\mathrm{E}\left[\delta\mathcal{E}\right] = \frac{C_s}{V}\mathrm{E}\left[\dot{z}^2\right] \tag{4}$$

where $\mathrm{E}\left[\cdot\right]$ denotes the operation of mathematical expectation. The mean-square of suspension motion can be determined in terms of properties of the stochastic input, namely roughness profile, using random vibrations theory. In what follows a brief review of the elements of this theory used in our model development is provided. Readers interested in more details are referred to classical textbooks on the subject (see e.g. Crandall and Mark (1963) and Lutes and Sarkani (1997)).

Elements of Random Vibration Theory

Stochastic Processes, Definition and Properties

Function $\xi(t)$ of an independent variable t is a random process, if $\xi(t_i)$ is a random variable for any value of t_i. Independent variable t can represent time or space for temporally or spatially varying stochastic processes. Moments of a stochastic process provide a great deal of information about its characteristics. The first moment is the mean $\mu_\xi(t) = \mathrm{E}[\xi(t)]$ and the second moment is the autocovariance function:

$$K_\xi(s,t) = \mathrm{E}[(\xi(t) - \mu_\xi(t))(\xi(s) - \mu_\xi(s))] \tag{5}$$

The autocorrelation function of a stochastic process, which is identical to the autocovariance function for zero-mean processes, is defined as:

$$R_\xi(s,t) = \mathrm{E}[\xi(t)\,\xi(s)] \tag{6}$$

A stationary random process has properties that are independent of the absolute time values; i.e. for the case of first two moments (so-called weakly stationary), the mean value does not depend on time ($\mu_\xi(t) = \mu$), and the autocorrelation function depends only on the time difference or lag ($R_\xi(s,t) = R_\xi(\tau = t - s)$). For a zero-mean stationary process the Wiener-Khintchine theorem (Khintchine (1934), Champeney (1987)) states that autocorrelation function $R_\xi(\tau)$ and power spectral density function $S_\xi(\omega)$ are Fourier transform pairs:

$$S_\xi(\omega) = \frac{1}{2\pi}\int_{-\infty}^{\infty} R_\xi(\tau)\exp(-i\omega\tau)\, d\tau \tag{7}$$

$$R_\xi(\tau) = \int_{-\infty}^{\infty} S_\xi(\omega)\exp(i\omega\tau)\, d\omega \tag{8}$$

where ω is the angular frequency. The power spectral density (PSD) of a stationary process which is truncated at $\pm T/2$ can also be expressed in terms of the Fourier transform of that process:

$$S_\xi(\omega) = \lim_{T\to\infty} \frac{2\pi}{T} \mathrm{E}\left[\left|\widehat{\xi}_T(\omega)\right|^2\right] \tag{9}$$

with $\widehat{\cdot}$ denoting Fourier transform. It can be shown that for any stochastic process $\xi(t)$, PSD function $S_\xi(\omega)$ is positive, real and even; hence it can also be specified as a one-sided function over only positive frequencies. Of special interest is the case where the time lag is $\tau = 0$ in Eq. (8), since this gives the mean-square of $\xi(t)$ as the area under its PSD:

$$\mathrm{E}\left[\xi^2(t)\right] = R_\xi(0) = \int_0^{\infty} S_\xi(\omega)\, d\omega \tag{10}$$

The stochastic process $\xi(t)$ is Gaussian (normal), if the random variables $\{\xi(t_i)\}_{i=1}^n$ are jointly Gaussian for any $n \in \mathbb{N}$ and all values of t_i. A stationary Gaussian process is completely characterized by its mean μ and autocorrelation function $R_\xi(\tau)$.

Response of a Linear Dynamical System to Random Excitations

Once the input excitation $\xi(t)$ to a linear system is decomposed into its harmonics via Fourier transformation, the steady-state response in frequency domain $\widehat{z}(\omega)$ can be expressed as:

$$\widehat{z}(\omega) = H_z(\omega)\,\widehat{\xi}(\omega) \tag{11}$$

where $H_z(\omega)$ is the frequency response function (FRS) defined as the ratio of input excitation $\xi(t)$ to output of interest $z(t)$ when input is the pure harmonic (i.e. when $\xi(t) = \exp(i\omega t)$). Frequency response function for derivatives of response is readily obtained from the frequency response function of the original response using the properties of Fourier transform of derivatives (i.e. $\widehat{dx(t)/dt} = i\omega\widehat{x}(\omega)$):

$$H_{\dot{z}}(\omega) = i\omega H_z(\omega) \tag{12}$$

Once FRS is known, the PSD of response can be related to the PSD of input excitation via:

$$S_z(\omega) = |H_z(\omega)|^2 S_\xi(\omega) \tag{13}$$

Roughness-Induced Dissipation in the Quarter-Car

For the 2-DOF quarter-car system in Figure 1 subjected to a displacement excitation $\xi(t)$ the equations of motion can be expressed in terms of the dimensionless parameters in Eq. (3) in the form:

$$\begin{bmatrix} 1 & 0 \\ 1 & \gamma \end{bmatrix} \begin{bmatrix} \ddot{y}_s \\ \ddot{y}_u \end{bmatrix} + 2\omega_s\zeta \begin{bmatrix} 1 & -1 \\ 0 & 0 \end{bmatrix} \begin{bmatrix} \dot{y}_s \\ \dot{y}_u \end{bmatrix} + \omega_s^2 \begin{bmatrix} 1 & -1 \\ 0 & \gamma\beta^2 \end{bmatrix} \begin{bmatrix} y_s \\ y_u \end{bmatrix} = \begin{bmatrix} 0 \\ 1 \end{bmatrix} \gamma\beta^2\omega_s^2\xi(t) \tag{14}$$

with y_s and y_u denoting the displacement of sprung and unsprung masses, respectively. In the presence of a pure harmonic input $\xi(t) = \exp(i\omega t)$ these displacement responses are expressed as $y_s = H_{y_s}(\omega)\exp(i\omega t)$ and $y_u = H_{y_u}(\omega)\exp(i\omega t)$. The frequency response functions are obtained by substituting these expressions in Eq. (14) and are of the form:

$$\begin{bmatrix} H_{y_s}(\omega) \\ H_{y_u}(\omega) \end{bmatrix} = \left(\begin{bmatrix} -\overline{\omega}^2 + \kappa & -\kappa \\ -\overline{\omega}^2 & -\overline{\omega}^2\gamma + \gamma\beta^2 \end{bmatrix} \right)^{-1} \begin{bmatrix} 0 \\ \gamma\beta^2 \end{bmatrix} \tag{15}$$

with $\kappa = 2i\overline{\omega}\zeta + 1$. The frequency response function of interest herein relates the relative displacement between the two masses $z = y_s - y_u$ to the input excitation in frequency domain (i.e. $\widehat{z}(\omega) = H_z(\omega)\,\widehat{\xi}(\omega)$), and is obtained from:

$$H_z(\omega) = H_{ys}(\omega) - H_{yu}(\omega) = \frac{-\overline{\omega}^2\gamma\beta^2}{\left(\overline{\omega}^2 - \kappa\right)\left(\overline{\omega}^2\gamma - \gamma\beta^2\right) - \overline{\omega}^2\kappa} \tag{16}$$

Using Eqs. (10), (11) and (12) the mean-square of suspension motion is expressed in terms of the frequency response function $H_z(\omega)$ and power spectral density of roughness $S_\xi(\omega)$:

$$\mathrm{E}\left[\dot{z}^2\right] = \int_0^\infty S_{\dot{z}}(\omega)\ d\omega = \int_0^\infty \omega^2 \left|H_z(\omega)\right|^2 S_\xi(\omega)\ d\omega \tag{17}$$

For a vehicle traveling with constant speed V the PSD of roughness $S_\xi(\omega)$ in function of the angular frequency relates to the PSD of roughness in function of the wave number $\Omega = \omega/V$ through $S_\xi(\Omega) = V S_\xi(\omega)$. The expected value of dissipation in Eq. (4) thus reads:

$$\mathrm{E}[\delta\mathcal{E}] = C_s V^{w-2} c \int_0^\infty \omega^{2-w} \left|H_z(\omega)\right|^2\ d\omega \tag{18}$$

or in the dimensionless functional form Eq. (3) expressed in terms of road roughness variables (c and w) as well as vehicle parameters (γ, β, and ζ):

$$\Pi = \frac{\mathrm{E}[\delta\mathcal{E}]}{m_s\omega_s^{4-w}V^{w-2}c} = 2\zeta \int_0^\infty \overline{\omega}^{2-w} \left|H_z(\overline{\omega})\right|^2\ d\overline{\omega} = F(\gamma, \beta, \zeta, w) \tag{19}$$

The result of the above analysis has two main practical applications. First, it provides a means to understand how roughness-induced dissipation scales with various vehicle and road parameters. Second, one can relate the above mechanistic model with mechanical-empirical models developed to estimate vehicle fuel consumption, such as calibrated HDM-4 model (Chatti and Zaabar, 2012). The insight gained from the mechanistic approach can be used to advance such models.

Relation with IRI

To achieve the above goals one important step is to establish a relationship between the dissipated energy and frequently used roughness metrics. It is common practice to capture road roughness through a single roughness index, such as the Average Rectified Slope (ARS), which is the accumulated suspension motion divided by the distance traveled, i.e. $\mathrm{ARS} = (VL)^{-1} \int_0^L |\dot{z}|\, dx$ (Sayers et al. (1986), Johannesson and Rychlik (2012)). For a specific quarter-car, the golden-car with properties shown in Table 1 traveling at a speed of $V_0 = 80$ km/h, ARS corresponds to the International Roughness Index (IRI). Here we assume that the road profile can be modeled via a zero-mean Gaussian process (Dodds and Robson (1973), ISO-8608 (1995), Sun et al. (2001)) – we comment later on how the results are affected if the road profile consists of bumps and valleys that cannot be captured by the "light" tails of a Gaussian distribution. Assuming a Gaussian marginal distribution for road profile, the absolute value of golden-car suspension motion $|\dot{z}|$ follows a folded normal distribution with mean $\sqrt{2\mathrm{E}\left[\dot{z}^2\right]/\pi}$ (Leone et al., 1961). The expected value of IRI thus reads:

$$\mathrm{E}\left[\mathrm{IRI}\right] = \frac{1}{V_0}\sqrt{\frac{2}{\pi}}\left[\int_0^\infty \omega^2 \left|H_{z-GC}\left(\omega\right)\right|^2 S_\xi\left(\omega\right)\, d\omega\right]^{1/2} \tag{20}$$

with subscript GC denoting that the quantity relates to the properties of the golden-car. The above equation can be expressed in terms of the PSD parameters:

$$\mathrm{E}\left[\mathrm{IRI}\right] = \left[\frac{2c}{\pi V_0^{3-w}} \int_0^{\infty} \omega^{2-w} \left|H_{z_{-GC}}\left(\omega\right)\right|^2 \, d\omega\right]^{1/2} \tag{21}$$

We note that IRI depends both on the golden-car dynamic properties (through frequency response function $H_{z_{-GC}}(\omega)$), and road roughness characteristics via roughness PSD parameters c and w. The above relation can be written in terms of the dimensionless variables defined in (3):

$$\mathrm{E}\left[\mathrm{IRI}\right] = \left[\frac{\omega_{s_{-GC}}^{3-w}}{V_0^{3-w}} \frac{\Pi_{GC}}{\pi \zeta_{GC}} c\right]^{1/2} = \alpha\sqrt{c} \tag{22}$$

The dimensionless dissipation of the golden-car, $\Pi_{GC} = \Pi(\gamma_{GC}, \beta_{GC}, \zeta_{GC})$ is evaluated from Eqs. (16) and (19) using the values given in Table 1. It only depends on the waviness number w, which typically varies between 1.5 and 3 (Kropac and Mucka (2004)). Specifically, for $w = 2$ as suggested by the International Standard Organization (ISO) (ISO-8608, 1995), the following relation between unevenness index c and IRI is obtained:

$$\mathrm{E}\left[\mathrm{IRI}\right] = \sqrt{\frac{\omega_{s_{-GC}}}{V_0} \frac{\Pi_{GC}}{\pi \zeta_{GC}} c} \tag{23}$$

which agrees with the expression $\mathrm{E}\left[\mathrm{IRI}\right]=2.21\sqrt{c}$ reported by Kropac and Mucka (2004) and Johannesson and Rychlik (2012). Finally, eliminating the unevenness index c between Eqs. (19) and (22), the expected value of dissipated energy is obtained in function of IRI and waviness number w:

$$\mathrm{E}\left[\delta\mathcal{E}\right] = k_d^2 m_s \omega_{s_{-GC}} \zeta_{GC} V_0 \left(\frac{V_0}{V}\right)^{2-w} \left(\frac{\omega_s}{\omega_{s_{-GC}}}\right)^{4-w} \frac{\Pi}{\Pi_{GC}} \mathrm{E}\left[\mathrm{IRI}\right]^2 \tag{24}$$

where $k_d = \sqrt{2}/\kappa$ with $\kappa = \mathrm{E}[|\dot{z}|]/\sqrt{\mathrm{E}[\dot{z}^2]}$. The coefficient k_d in the above equation depends on the marginal distribution of the suspension motion process and is equal to π when the road profile (and consequently the suspension motion) follows a Gaussian distribution. Other forms of distributions will be addressed later on.

Scaling of Energy Dissipation

We are interested in the scaling of energy dissipation with different vehicle and road properties.

Scaling with road condition: The expected value of dissipation is proportional to $\mathrm{E}[\mathrm{IRI}]^2$. For a specific vehicle (i.e. constant values of β, γ and ζ) the ratio of dimensionless dissipation Π/Π_{GC} only depends on w, and decreases as w increases. Figures 2 and 3 show the variation of this dimensionless ratio as a function of w for different values of β, γ. The dissipation also scales with vehicle speed as V^{w-2} which indicates that dissipation increases with speed if $w > 2$, decreases with speed if $w < 2$ and is independent of speed when $w = 2$.

Scaling with vehicle properties: For fixed road condition (i.e. fixed values of IRI and w), the dissipation scales according to Eq. (24), with vehicle sprung mass m_s and the corresponding natural frequency as ω_s^{4-w}. Our parametric studies show that the roughness-induced dissipation does not change significantly with variation in the dimensionless damping ratio ζ, and therefore it is disregarded in the analysis. The ratio of dimensionless dissipation Π/Π_{GC} in functions of the two vehicle specific invariants β and γ shown in Figure 4 reveals that for a specific road condition, the dimensionless dissipation increases with both β and γ.

Special case $w = 2$**:** For the special case of $w = 2$ one can express the dimensionless dissipation in function of dimensionless invariants γ and β:

$$\Pi = \frac{\pi\gamma\beta^2}{2} \tag{25}$$

Therefore the roughness-induced dissipation reduces to:

$$\mathrm{E}\left[\delta\mathcal{E}\right] = m_s\omega_s^2 c\frac{\pi\gamma\beta^2}{2} = \frac{\pi c}{2}k_t \tag{26}$$

That is, for a specific road roughness, the dissipation only depends on tire stiffness, k_t.

IMPACT OF MARGINAL PROBABILITY DENSITY FUNCTION: NON-GAUSSIAN BUMPS AND VALLEYS

Here we discuss how the results presented in previous section are affected if the road profile data exhibits bumps and valleys that are not captured by the "light" tails of a Gaussian distribution. In fact, there is evidence that non-Gaussian distributions with heavier tails are better suited for modeling the frequency of observed values in road elevation profile data, especially when the phenomenon to be examined is analyzed for longer sections of the road profile (Bruscella et al. (1999), Steinwolf and Connon (2005), Johannesson and Rychlik (2013)). For example, Bruscella et al. (1999) analyzed several hundred kilometers of Victorian (Australia) road profile data, and observed that the normalized histogram of the elevation profile has heavier tails compared to that of a Gaussian distribution. Figure 5 shows the empirical probability distribution function (PDF) associated with the data reported in this study against a Gaussian distribution with the same mean and variance in both linear and logarithmic scales. Deviation from Gaussian assumption is evident indicating that the road profile needs to be modeled as a non-Gaussian stochastic process. In fact using a

Gaussian distribution to model marginal distribution of the elevation profile in such cases results in the loss of statistically uncommon events and extreme values (e.g. elevations exceeding ± 3 standard deviation pertaining to, for example, faulting).

A natural way to relax the Gaussian assumption and enrich the modeling process by incorporating distributions of the type shown in Figure 5 where the lack of shoulders and heavy tails are the main attributes, is to use probability distributions with higher kurtosis. Kurtosis, defined as the ratio of fourth central moment to the square of the variance ($\beta_2 = \mu_4/\mu_2^2$, with μ_n the n^{th} central moment), is a measure of tail weight and peakedness in a distribution (with higher kurtosis representing heavier tails and more peakedness). It represents a movement of probability mass that does not affect the variance. It is thus instructive to compare the empirical probability density function of road profile data to distributions which look similar to the Gaussian distribution but have heavier tails and higher peaks, and choose a distribution that best fits the profile data. Figure 6 illustrates PDF of the road profile examined by Bruscella et al. (1999) along with Gaussian distribution ($\beta_2 = 3$) and three non-Gaussian but symmetric distributions, i.e. logistic distribution, hyperbolic secant distribution and Laplace distribution, each having kurtosis equal to 4.2, 5 and 6 respectively. It is observed that PDF of the road profile matches closely a Laplace distribution which has the heaviest tails among the three distributions.

Adopting a non-Gaussian distribution to describe the road profile data the scaling relationships previously derived need to be revisited. This is achieved by using a simulation framework that allows the generation of realizations from a non-Gaussian random process given its power spectral density (c and w in our case) and marginal distribution. Once such realizations of the road profile are available they are fed into the golden-car model to obtain realizations of IRI. The functional relationship between c and IRI is then numerically determined by averaging over multiple runs, with each run simulating the dynamics of the golden-car run over a single realization of the road profile.

Translation Process Theory

Realizations of the road profile are generated based on the translation process theory introduced by Nataf (1962) and later developed by Grigoriu (1984), Liu and Der Kiureghian (1986) and Grigoriu (1998). A nonlinear transformation of the form:

$$Y(s) = F_Y^{-1}\left(\Phi\left(X(s)\right)\right) \tag{27}$$

with $X(s)$ a standard stationary Gaussian process, is used to model a stationary non-Gaussian process $Y(s)$. Herein, $F_Y(y)$ is the (target) marginal cumulative distribution function of the process $Y(s)$, and Φ represents the standard Gaussian cumulative distribution function. It can been shown that the autocorrelation function of the resulting non-Gaussian process $R_Y(\tau)$ is related to the autocorrelation function of the underlying Gaussian process $R(\tau)$ by (Grigoriu (1998)):

$$R_Y(\tau) = \int_{-\infty}^{\infty}\int_{-\infty}^{\infty} F_Y^{-1}\left(\Phi(x_1)\right) F_Y^{-1}\left(\Phi(x_2)\right) \phi\left(x_1, x_2, \rho(\tau)\right) dx_1 dx_2 \tag{28}$$

with $\rho(\tau) = R(\tau)/\sigma^2$ and ϕ the bivariate Gaussian probability density function. Generating realizations of the non-Gaussian process then boils down to: (i) finding the autocorrelation function $R(\tau)$ of the Gaussian process given the target autocorrelation function or PSD (note these two are directly related). This is achieved by numerically inverting Eq. (28) provided the target marginal CDF and autocorrelation functions are "compatible", or by means of iterative schemes that converge toward the best match for the autocorrelation function or the associated PSD (see Grigoriu (1998) or Shields et al. (2011)); (ii) generating samples of the Gaussian process using one of the available techniques (see e.g. Shinozuka and Deodatis (1991) and Grigoriu (1993)); and (*iii*) using the nonlinear transformation Eq. (27) to generate samples of the non-Gaussian process.

Impact on Scaling Relations

A total of 5,000 road profile realizations were generated from a stochastic process with Laplace marginal distribution and roughness PSD function $S_\xi = c\Omega^{-w}$. Two sample profiles are illustrated in Figure 7 along with their Gaussian counterparts. The profiles with marginal Laplace distributions have more observable bumps and extremes compared to the ones with Gaussian distribution. The response, i.e. suspension motion of the golden-car, $\dot{z}$, due to road roughness is then evaluated by solving the equations of motion Eq. (14) for each of these realizations. The average IRI of simulated profiles is evaluated and plotted in function of c in Figure 8 for a wide range of unevenness index c that covers the range of IRI values in practice. While scaling with IRI of the unevenness index remains constant, the multiplicative factor α in the functional relationship (22) changes. We also included the $c-$ IRI curves obtained by approximating the marginal PDF of the suspension motion process by the same family of distributions as the one used in describing the road profile elevation. The curve associated with logistic distribution is, for example, obtained assuming the following distribution of $\dot{z}$:

$$f\left(\dot{z}\right) = \frac{1}{4s}\text{sech}^2\left(\frac{\dot{z}-\mu_{\dot{z}}}{2s}\right) \tag{29}$$

where $\mu_{\dot{z}}$ is the mean value and $s = \sqrt{3}\sigma_{\dot{z}}/\pi$ with $\sigma_{\dot{z}}$ standard deviation of $\dot{z}$. The absolute value of response $Y = |\dot{z}|$ has then a folded logistic distribution with the following CDF:

$$F_Y\left(y\right) = \frac{1}{1+\exp\left(-\frac{y-\mu_{\dot{z}}}{s}\right)} + \frac{1}{1+\exp\left(-\left(\frac{y+\mu_{\dot{z}}}{s}\right)\right)} - 1 \tag{30}$$

For the special case of zero-mean $\dot{z}$, one can readily show that $E\left[|\dot{z}|\right] = 2s\ln 2$. Eqs. (21) and (22) can thus be rewritten as follows:

$$\mathrm{E}\left[\mathrm{IRI}\right] = \frac{2\ln 2}{\pi}\left[\frac{3c}{V_0^{3-w}}\int_0^{\infty}\omega^{2-w}\left|H_z\left(\omega\right)\right|^2\, d\omega\right]^{1/2} = \frac{\ln 2}{\pi}\left[c\frac{6\omega_s^{3-w}}{V_0^{3-w}}\frac{\Pi_{GC}}{\zeta_{GC}}\right]^{1/2} \tag{31}$$

Table 2 summarizes the result of similar calculations for different distributions of the marginal PDF of the suspension motion. Numbers associated with a Gaussian marginal PDF are also included for the sake of comparison. As shown in Figure 8 the hyperbolic secant distribution provides the best approximation for the functional relationship between unevenness index c and IRI. This can be explained by carefully examining the marginal distribution of suspension response. In fact, Figures 9 and 10 depict this distribution for waviness number $w = 2.5$ and different values of unevenness index c plotted against the associated Gaussian, Laplace, hyperbolic secant and logistic distributions. It is observed that the marginal PDF of response has heavier tails than that of a Gaussian distribution. This is manifested in a higher kurtosis value of 4.85 as compared to that of a Gaussian distribution, 3. Comparing the marginal PDF of $\dot{z}$ to three different non-Gaussian PDFs, one also observes that the marginal distribution of suspension motion process is very close to hyperbolic secant distribution.

APPLICATION: HANDSHAKE WITH HDM-4 MODEL

The framework developed herein relates road surface characteristics and dynamic properties of a quarter-vehicle to the roughness-induced dissipation, and thus fuel consumption. In practice, however, vehicle dynamics is far more complex than the simplified quarter-car model. In addition, measuring all dynamic properties of vehicle with a reasonable accuracy may not be always feasible. For instance, while it is possible to measure the inertial properties (sprung and unsprung masses) accurately, the total stiffness involved in different parts of a vehicle is more complicated than stiffness of suspension and tire and may be very hard to measure. In the absence of such detailed measurements empirical models such as the HDM-4 model (Zaabar and Chatti (2010)) can be used to calibrate the proposed roughness-induced mechanistic model. In such a calibration, the stiffness properties for different classes of vehicles, together with the road waviness number as an additional adjustable parameter are estimated (Louhghalam et al. (2014a)). The HDM-4 model reports the variation of excess fuel consumption due to change in IRI at different vehicle speeds and for five classes of vehicle: medium car, SUV, van, light truck and heavy truck.

To calibrate the mechanistic model, the dissipated energy is first converted to fuel consumption using engine efficiency coefficient (ξ_b in mL/kW/s). The calibration parameters, i.e. stiffness properties of each vehicle class and a single road waviness number, are then determined by minimizing the difference between two model predictions of change in fuel consumption. Calibration is performed for practical ranges of IRI and vehicle speed, corresponding to the field measurements in Chatti and Zaabar (2012). A detailed description of the calibration procedure is explained in Louhghalam et al. (2014a), where the marginal distribution of road profile was assumed to be Gaussian (see Table 3 for a summary of results). The results of our calibrated model are illustrated in Figure 11 for vehicle speeds 70 and 100 km/h and compared with the predictions of calibrated HDM-4 model (Chatti and Zaabar (2012)). The plots show the change in total fuel consumption in function of IRI for five vehicle classes. In contrast to the HDM-4 model, where fuel consumption is linearly related to IRI, the developed mechanistic model establishes a quadratic relation between energy dissipation and IRI. It is worth noting that the HDM-4 model for estimating roughness-induced fuel consumption is an empirical model where a functional relationship, presumed to be varying linearly with IRI, is fitted to the experimental measurements. Hence the scaling in IRI is assumed a priori and is not the result of dynamic analysis of road roughness-vehicle interaction. The calibration parameters can also be determined if the Gaussian assumption for profiles is relaxed. Table 3 also shows the stiffness parameters for the three non-Gaussian distributions discussed before. The waviness number w =2.4117 is the same for all distributions studied, which agrees well with the results of statistical analysis of the Long-Term Pavement Performance program of the US Federal Highway Administration (FHWA) reported by Kropac and Mucka (2008), exhibiting a mode at around $w = 2.5$.

CONCLUDING REMARKS

The mechanistic model developed in this paper quantifies the impact of road roughness characteristics on vehicle fuel consumption as one of the sources of energy dissipation related to rolling resistance. Such models are necessary for assessing the environmental footprint of pavement structures during their use phase, thus contributing to the emerging quantitative framework of engineering sustainability. The unique feature of this model is that it integrates the uncertainty in pavement profiles into a thermodynamic quantity (energy dissipation) using random vibration techniques. This provides a means to identify the governing parameters that drive roughness-induced dissipation and related excess fuel consumption.

The results of our analysis establish the relationship between the statistical characteristics of road profile and vehicle dynamic properties and energy dissipation. The scaling of dissipation with IRI proposed by the mechanistic model (i.e. $\delta\mathcal{E} \propto \mathrm{IRI}^2$) is different from the linear scaling of dissipation with IRI reported by empirical models such as HDM-4. In our mechanistic model the road roughness is represented by two independent parameters, IRI and w. This is in contrast with empirical models in which only IRI is normally used to represent the road surface condition.

Furthermore, for a specific vehicle, scaling of the dissipated energy with speed varies with the waviness number as $\mathrm{E}[\delta\mathcal{E}] \propto V^{w-2}$. This implies that the dissipation increases with speed for $w > 2$, and for $w < 2$ it is the inverse. In return, since the waviness number of pavements varies in the range $w = 2.5 \pm 0.5$, the variation of speed does not change the roughness-induced dissipation significantly. For instance, for $w = 2.41$ obtained from calibration, increasing the speed by 100 % results in only 33 % increase in dissipation. In other words, the variation of fuel consumption due to change of speed should generally not be attributed to roughness-induced dissipation.

When Gaussian distributions fail to represent the frequency of extreme values and bumps in the road, the found scaling relationships of energy dissipation with road surface parameters and vehicle dynamic properties remain unchanged. In return, all what changes is the multiplicative factor in the functional form relating energy dissipation and these parameters and properties.

ACKNOWLEDGMENT

This research was carried out by the CSHub@MIT with sponsorship provided by the Portland Cement Association (PCA) and the Ready Mixed Concrete (RMC) Research & Education Foundation. The CSHub@MIT is solely responsible for content.

REFERENCES

Akbarian, M., Moeini-Ardakani, S. S., Ulm, F.-J., and Nazzal, M. (2012). "Mechanistic approach to pavement-vehicle interaction and its impact on life-cycle assessment." *Transportation Research Record: Journal of the Transportation Research Board*, 2306(1), 171–179.

Beuving, E., De Jonghe, T., Goos, D., Lindahl, T., and Stawiarski, A. (2004). "Fuel efficiency of road pavements." *Proceedings Of The 3rd Eurasphalt and Eurobitume Congress Held Vienna, May 2004*, Vol. 1.

Bruscella, B., Rouillard, V., and Sek, M. (1999). "Analysis of road surface profiles." *Journal of Transportation Engineering*, 125(1), 55–59.

Buckingham, E. (1914). "On physically similar systems; illustrations of the use of dimensional equations." *Physical Review*, 4(4), 345–376.

Champeney, D. C. (1987). *A handbook of Fourier theorems.* Cambridge University Press.

Chatti, K. and Zaabar, I. (2012). *Estimating the effects of pavement condition on vehicle operating costs, Project 1-45.* National Cooperative Highway Research Program, Report 720.

Crandall, S. H. and Mark, W. D. (1963). *Random vibration in mechanical systems.* Academic Press.

Dastun1200 (accessed 2013). "Spring rate., <`http://datsun1200.com/modules/mediawiki/index.php?title=Spring_Rates`>.

Dixon, J. C. (1996). *Tires, suspension, and handling.* Society of Automotive Engineers Warrendale, PA.

Dodds, C. and Robson, J. (1973). "The description of road surface roughness." *Journal of Sound and Vibration*, 31(2), 175–183.

Fancher, P. S. (1986). "A factbook of the mechanical properties of the components for single-unit and articulated heavy trucks. phase i. final report.

Flintsch, G. W., de León, E., McGhee, K. K., and AI-Qadi, I. L. (2003). "Pavement surface macrotexture measurement and applications." *Transportation Research Record: Journal of the Transportation Research Board*, 1860(1), 168–177.

Grigoriu, M. (1984). "Crossings of non-gaussian translation processes." *Journal of Engineering Mechanics*, 110(4), 610–620.

Grigoriu, M. (1993). "Simulation of stationary process via a sampling theorem." *Journal of sound and vibration*, 166(2), 301–313.

Grigoriu, M. (1998). "Simulation of stationary non-gaussian translation processes." *Journal of engineering mechanics*, 124(2), 121–126.

ISO-8608 (1995). "Mechanical vibration – road surface profiles – reporting measured data." *ISO*, 8608: 1995(E).

Johannesson, P. and Rychlik, I. (2012). "Modeling of road profiles using roughness indicators.

Johannesson, P. and Rychlik, I. (2013). "Laplace processes for describing road profiles." *Procedia Engineering*, 66, 464–473.

Khintchine, A. (1934). "Korrelationstheorie der stationären stochastischen prozesse." *Mathematische Annalen*, 109(1), 604–615.

Kropac, O. and Mucka, P. (2004). "Non-standard longitudinal profiles of roads and indicators for their characterisation." *International journal of vehicle design*, 36(2), 149–172.

Kropac, O. and Mucka, P. (2008). "Indicators of longitudinal unevenness of roads in the usa." *International Journal of Vehicle Design*, 46(4), 393–415.

Leone, F., Nelson, L., and Nottingham, R. (1961). "The folded normal distribution." *Technometrics*, 3(4), 543–550.

Liu, P.-L. and Der Kiureghian, A. (1986). "Multivariate distribution models with prescribed marginals and covariances." *Probabilistic Engineering Mechanics*, 1(2), 105–112.

Louhghalam, A., Akbarian, M., and Ulm, F.-J. (2013). "Flügge's conjecture: Dissipation vs. deflection induced pavementvehicleinteractions (pvi)." *Journal of Engineering Mechanics*.

Louhghalam, A., Akbarian, M., and Ulm, F.-J. (2014a). "Roughness-induced pavement-vehicle interactions: Key parameters and impact on vehicle fuel consumption." *Transportation Research Record: Journal of the Transportation Research Board*, accepted.

Louhghalam, A., Akbarian, M., and Ulm, F.-J. (2014b). "Scaling relations of dissipation-induced pavement-vehicle interactions." *Transportation Research Record: Journal of the Transportation Research Board*, accepted.

Lutes, L. D. and Sarkani, S. (1997). *Stochastic analysis of structural and mechanical vibrations*. Prentice Hall Englewood Cliffs, NJ.

Nataf, A. (1962). "Statistique mathematique-determination des distributions de probabilites dont les marges sont donnees." *Comptes Rendus Hebdomadaires Des Seances De L Academie Des Sciences*, 255(1), 42.

Pouget, S., Sauzéat, C., Benedetto, H. D., and Olard, F. (2011). "Viscous energy dissipation in asphalt pavement structures and implication for vehicle fuel consumption." *Journal of Materials in Civil Engineering*, 24(5), 568–576.

Robson, J. (1979). "Road surface description and vehicle response." *International Journal of Vehicle Design*, 1(1).

Sandberg, U., Bergiers, A., Ejsmont, J. A., Goubert, L., Karlsson, R., and Zöller, M. (2011). "Road surface influence on tyre/road rolling resistance." *Swedish Road and Transport Research Institute (VTI). Prepared as part of the project MIRIAM, Models for rolling resistance In Road Infrastructure Asset Management systems. Available on the World Wide Web:¡ http://www. miriam-co2. net/Publications/MIRIAM_SP1_Road-Surf-Infl_Report*, 20111231.

Sayers, M. W. (1995). "On the calculation of international roughness index from longitudinal road profile." *Transportation Research Record*, 1501, 1–12.

Sayers, M. W., Gillespie, T. D., and Queiroz, A. (1986). "The international road roughness experiment. establishing correlation and a calibration standard for measurements." *Report no.*

Shields, M., Deodatis, G., and Bocchini, P. (2011). "A simple and efficient methodology to approximate a general non-gaussian stationary stochastic process by a translation process." *Probabilistic Engineering Mechanics*, 26(4), 511–519.

Shinozuka, M. and Deodatis, G. (1991). "Simulation of stochastic processes by spectral representation." *Applied Mechanics Reviews*, 44(4), 191–204.

Steinwolf, A. and Connon, W. H. (2005). "Limitations of the fourier transform for describing test course profiles." *Sound and Vibration*, 39(2), 12–17.

Sun, L., Zhang, Z., and Ruth, J. (2001). "Modeling indirect statistics of surface roughness." *Journal of transportation engineering*, 127(2), 105–111.

Winkler, C. B. (1983). “Evaluation of barrier limit capacity for different classes of vehicles and impact conditions-parameter measurements of: 1982 chevrolet s-10 pickup, 1982 chevrolet c-10 pickup, 1982 ford f-150 van. final report.

Zaabar, I. and Chatti, K. (2010). “Calibration of hdm-4 models for estimating the effect of pavement roughness on fuel consumption for us conditions.” *Transportation Research Record: Journal of the Transportation Research Board*, 2155(1), 105–116.

LIST OF FIGURES

and 100 km/h for (a): Medium car (b): SUV (c): Van (d):Light truck (e): Articulated truck

List of Tables

TABLE 1: Properties of the golden-car (data from Sayers (1995))

Property	Value	Units
k_t/m_s	653	[s^{-2}]
k_s/m_s	63.3	[s^{-2}]
C_s/m_s	6.0	[s^{-1}]
m_u/m_s	0.15	[1]

TABLE 2: Values of α in $E\left[\mathrm{IRI}\right] = \alpha\sqrt{c}$ and k_d in Eq. (24) for various distributions

Probability distribution	α	k_d
Gaussian	1.9154	$\sqrt{\pi}$
Logistic	1.8348	$\pi/\sqrt{6}\ln 2$
Hyperbolic Secant	1.7823	$\sqrt{2}\pi^2/7.328$
Laplace	1.6975	2

TABLE 3: Vehicle dynamic properties per axel

Vehicle class	Medium car	SUV	Van	Light truck	Articulated truck
Total mass, m_t (tons)	1.46[1]	2.5[1]	2.54[1]	6.5[1]	34.9[1]
Unsprung mass, m_u (kg)	80[2]	125[3]	134[7]	395[5]	544[6]
Suspension stiffness k_s (kN/m)	29.44[2]	189[3]	48[4]	337[5]	700[6]
Fuel efficiency coefficient ξ_b (mL/kW/s)	.096[1]	.072[1]	.072[1]	.062[1]	.059[1]
β (Gaussian)	46.98	28.03	31.00	14.90	13.30
β (Logistic)	44.46	26.51	29.32	13.95	12.54
β (Hyperbolic secant)	42.84	25.53	28.24	13.42	12.04
β (Laplace)	40.24	23.95	26.51	12.57	11.26

1 - Chatti and Zaabar (2012)
2 - Dixon (1996)
3 - CarSim template
4 - Dastun1200 (2013)
5 - GMC Specification manual
6 - Fancher (1986)
7 - Winkler (1983)

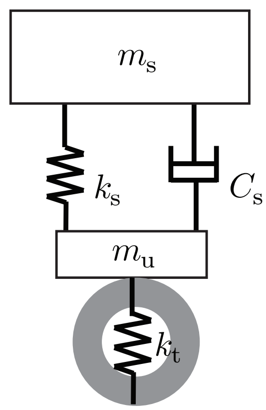

FIG. 1: Quarter-Car model adapted from Sayers (1995)

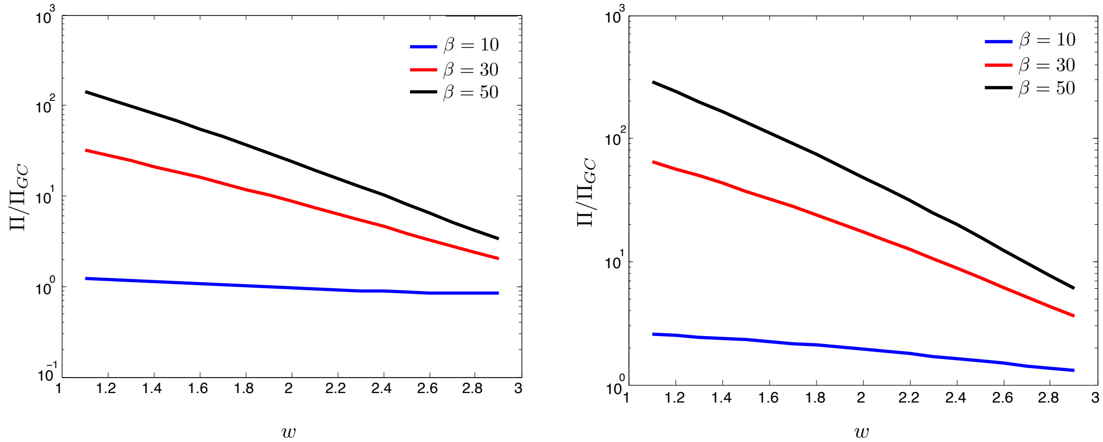

(a) $\gamma = 0.1$ (b) $\gamma = 0.2$

FIG. 2: Ratio of dimensionless dissipation Π/Π_{GC} versus waviness number w for different β values at (a): $\gamma = 0.1$ (b): $\gamma = 0.2$

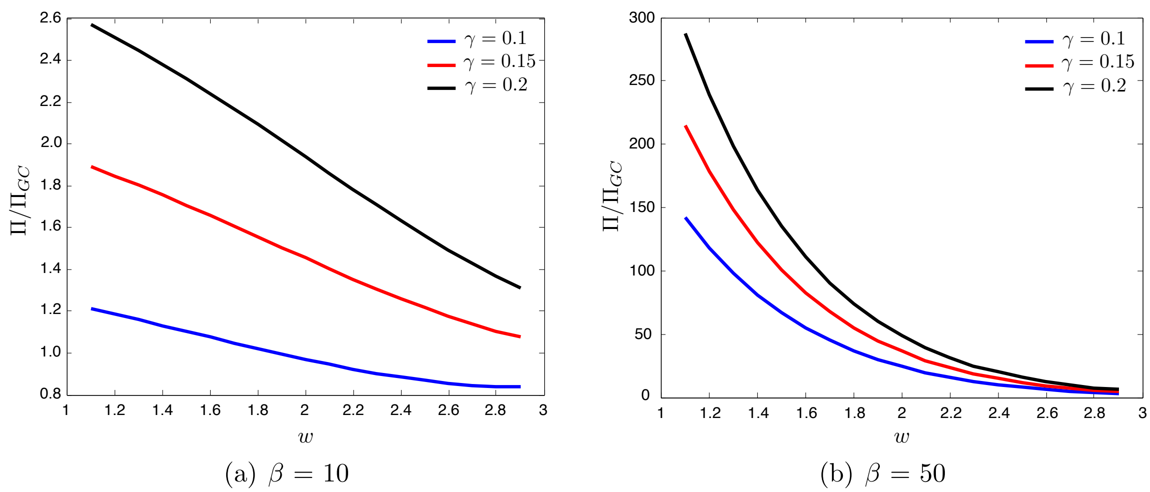

FIG. 3: Ratio of dimensionless dissipation Π/Π_{GC} versus waviness number w for different γ values at (a): $\beta = 10$ (b): $\beta = 50$

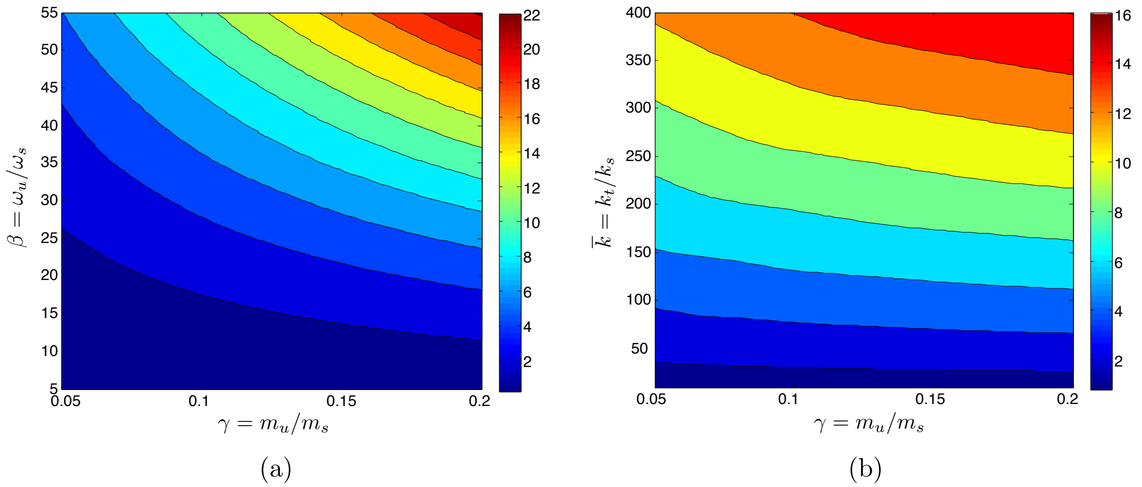

FIG. 4: Ratio of dimensionless dissipation Π/Π_{QC} in function of (a): γ and β (b): γ and k_t/k_s

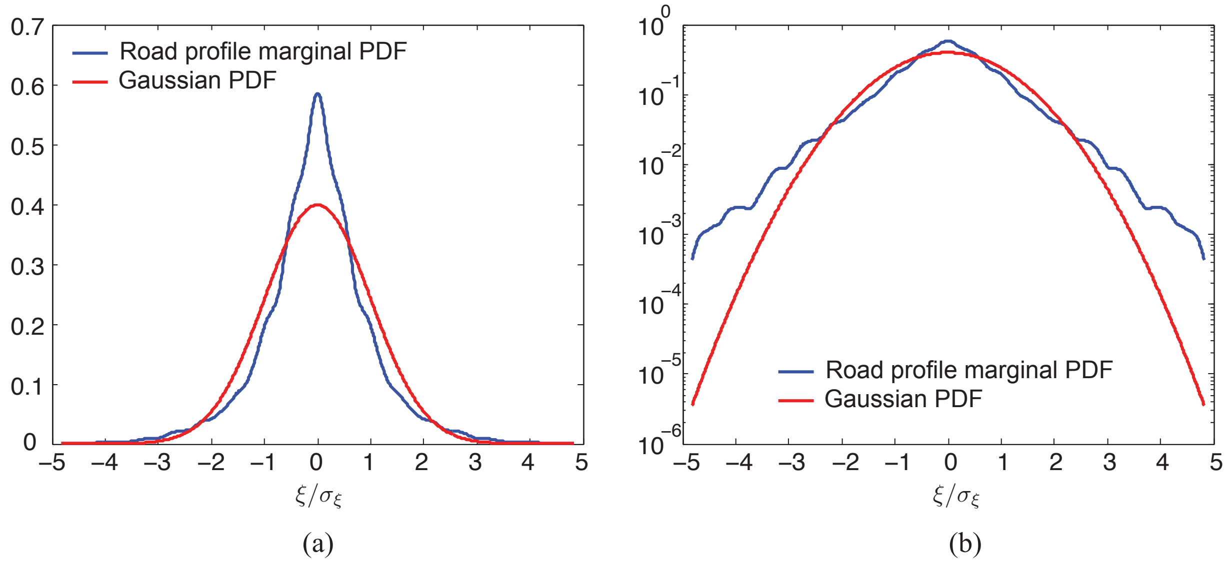

FIG. 5: PDF of road profiles adapted from Bruscella et al. (1999) and the associated normal distribution in (a): linear scale (b): logarithmic scale; the tails of the of empirical distribution are heavier than that of the associated Gaussian distribution

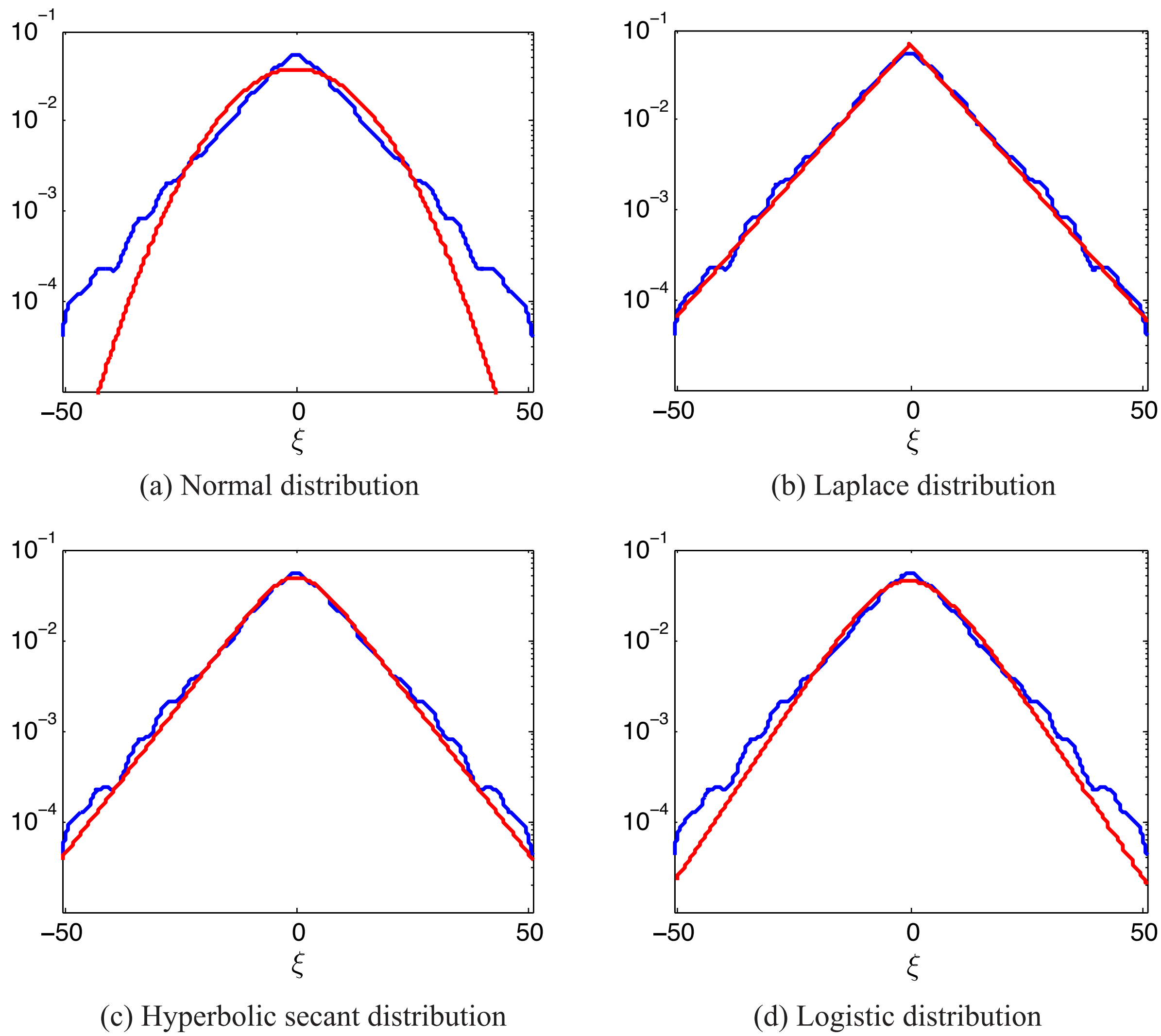

FIG. 6: PDF of road roughness adapted from Bruscella et al. (1999) and the associated (a): Gaussian distribution (b): Laplace distribution (c): hyperbolic secant distribution (d): logistic distribution

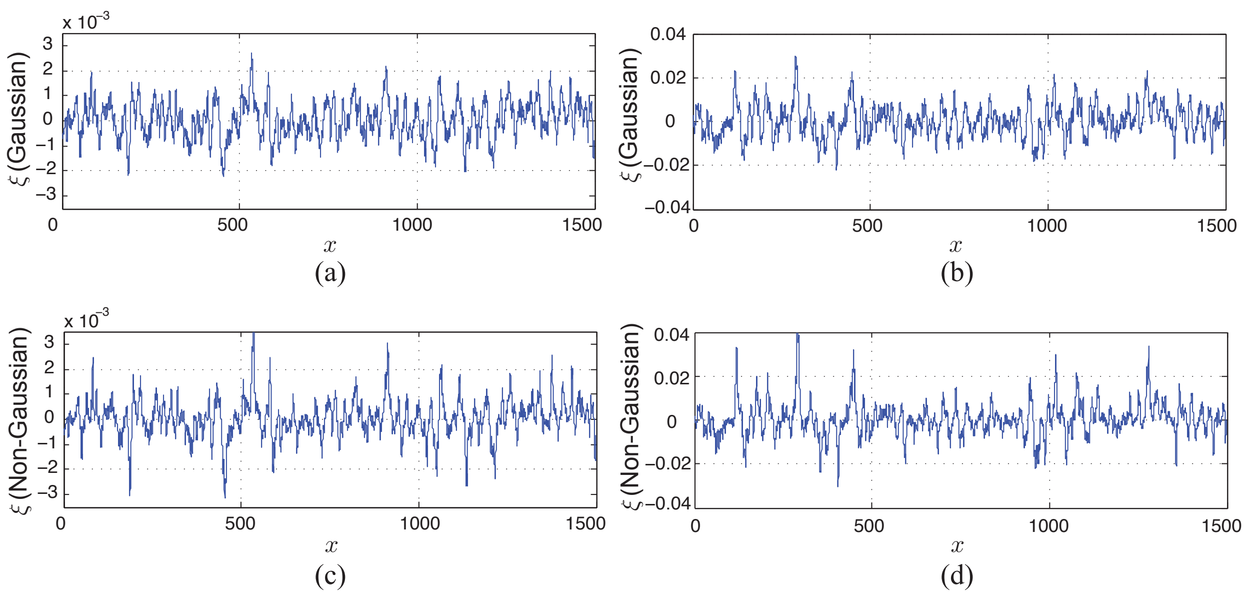

FIG. 7: Simulated roughness profiles with (a): Gaussian distribution ($c = 3.16 \times 10^{-8}$) (b): Gaussian distribution ($c = 3.16 \times 10^{-6}$) (c): Laplace distribution ($c = 3.16 \times 10^{-8}$) (d): Laplace distribution ($c = 3.16 \times 10^{-6}$)

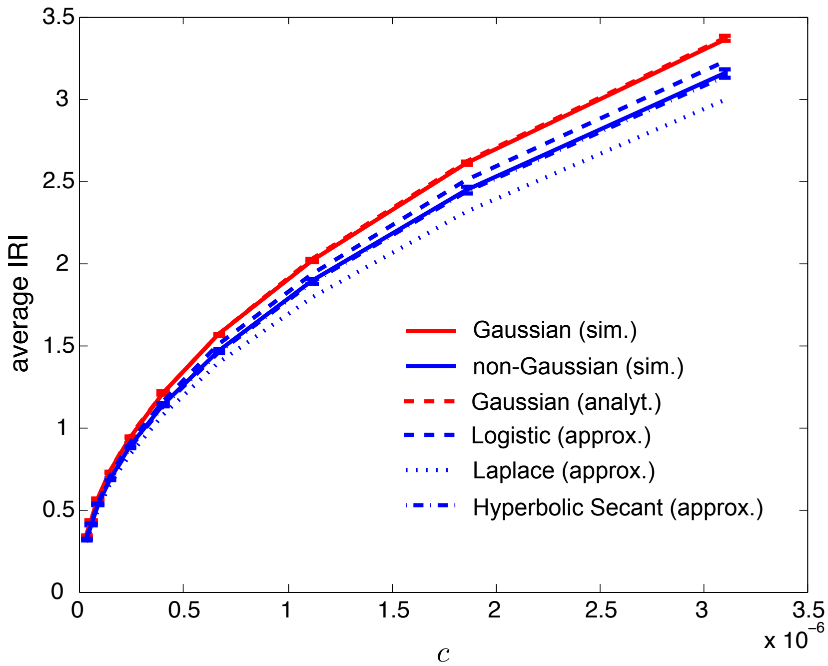

FIG. 8: International roughness index in function of unevenness index, c, for $w = 2.5$

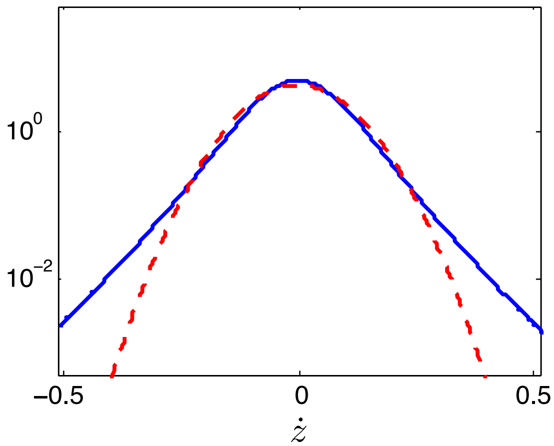

(a) Normal distribution

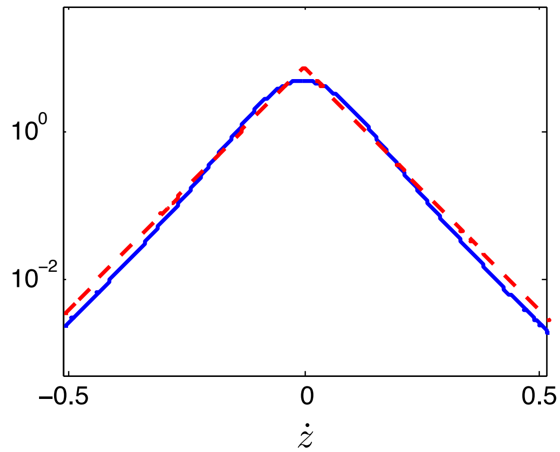

(b) Laplace distribution

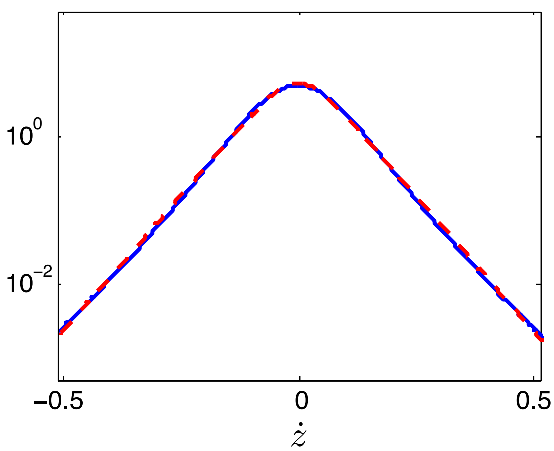

(c) Hyperbolic secant distribution

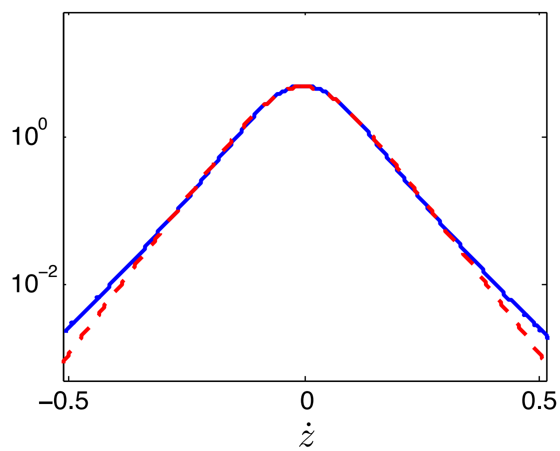

(d) Logistic distribution

FIG. 9: PDF of suspension motion $\dot{z}$ due to roughness with Laplace distribution and unevenness number $c = 3.16 \times 10^{-6}$ along with its associated (a): Gaussian distribution (b): Laplace distribution (c): hyperbolic secant distribution (d): logistic distribution

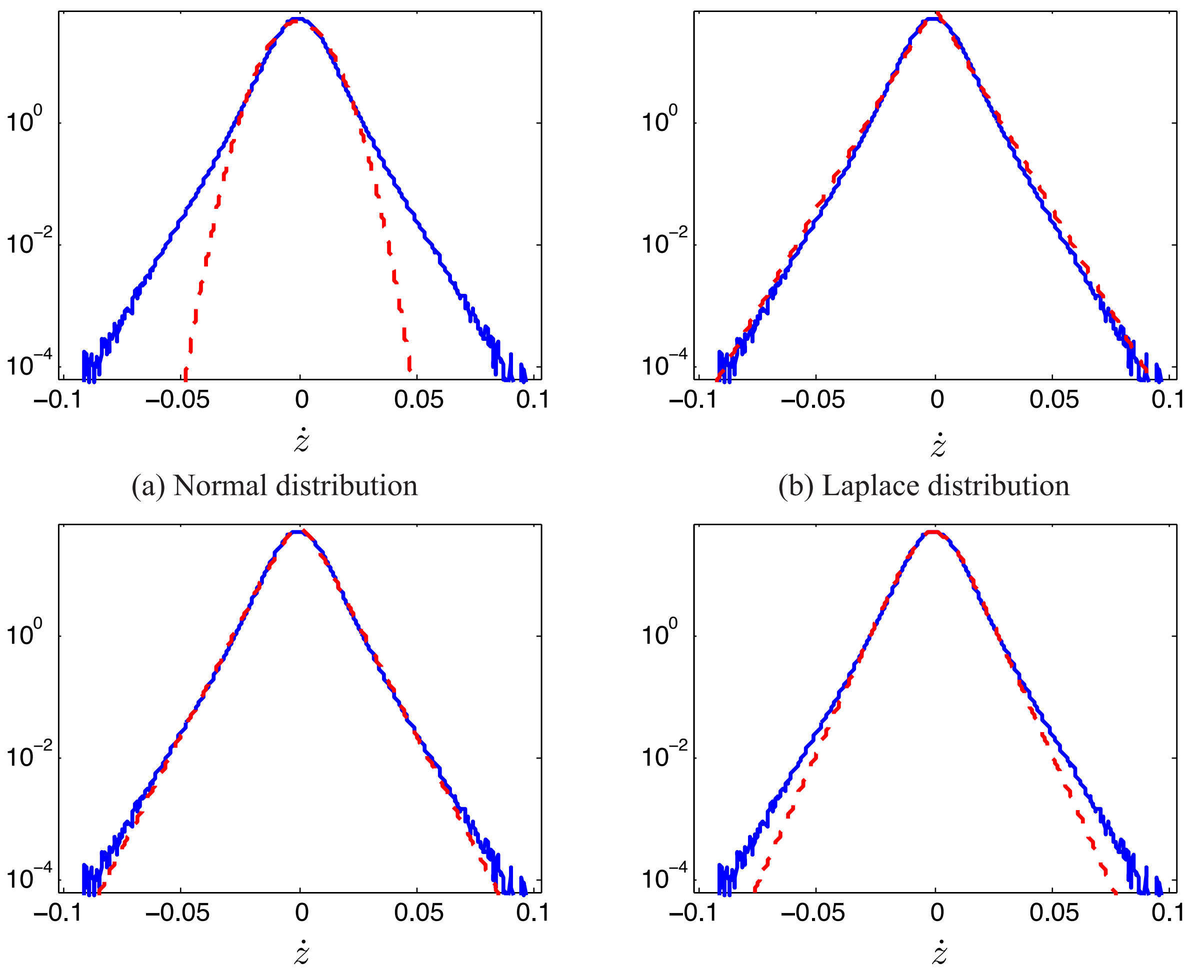

(a) Normal distribution (b) Laplace distribution (c) Hyperbolic secant distribution (d) Logistic distribution

FIG. 10: PDF of suspension motion $\dot{z}$ due to roughness with Laplace distribution and unevenness number $c = 3.16 \times 10^{-8}$ along with its associated (a): Gaussian distribution (b): Laplace distribution (c): hyperbolic secant distribution (d): logistic distribution

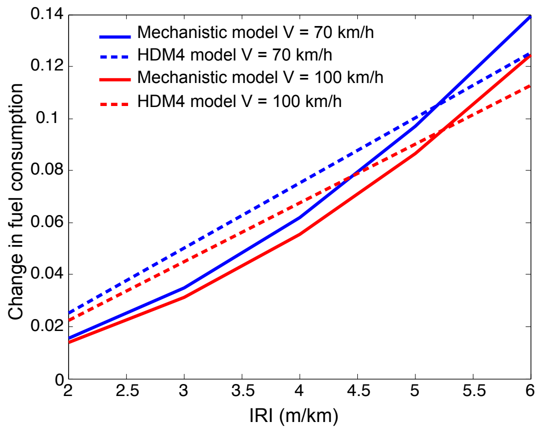

(a) Medium Car

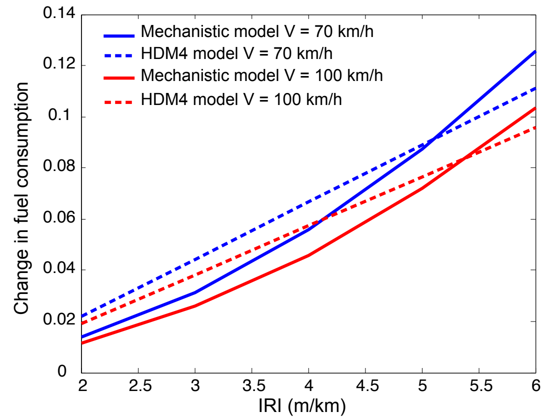

(b) SUV

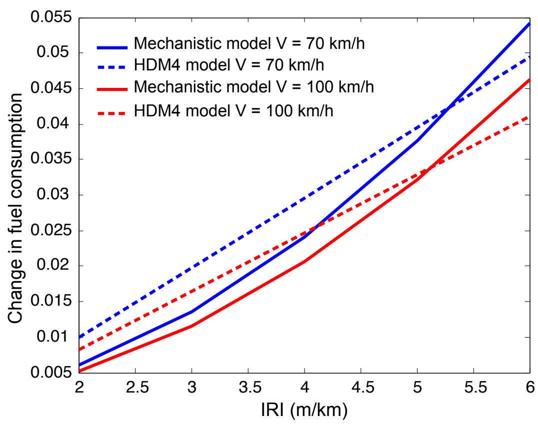

(c) Van

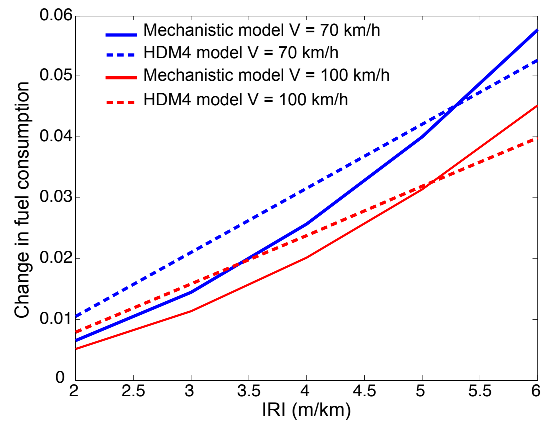

(d) Light Truck

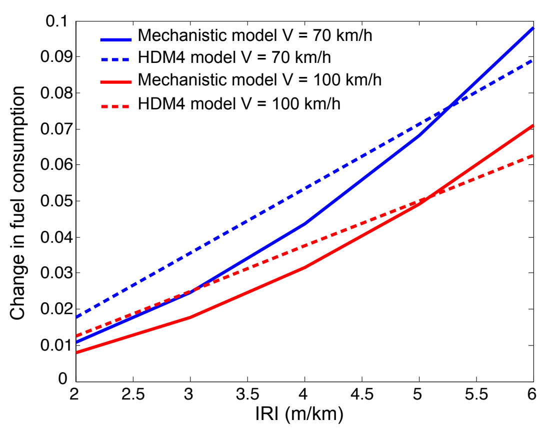

(e) Articulated Truck

FIG. 11: Change in roughness-induced excess fuel consumption in function of IRI at $V =$ 70 and 100 km/h for (a): Medium car (b): SUV (c): Van (d):Light truck (e): Articulated truck